Journal of Organometallic Chemistry 892 (2019) 34–40

Contents lists available at ScienceDirect

Journal of Organometallic Chemistry

journal homepage: www.elsevier.com/locate/jorganchem

Study on synthesis, characterization, and nonvolatile memory behavior of ferrocene-containing metallopolymers

Xiaozhe Cheng [a, 1], Asaduzzaman Md [b, 1], Hong Lian [a], Zheng Zhong [a], Hongen Guo [a], Qingchen Dong [a, *], V.A.L. Roy [b, **]

[a] Ministry of Education Key Laboratory of Interface Science and Engineering in Advanced Materials, Research Center of Advanced Materials Science and Technology, Taiyuan University of Technology, Taiyuan, 030024, China
[b] State Key Laboratory for THz and Millimeter Waves and Department of Materials Science & Engineering, City University of Hong Kong, Tat Chee Avenue, Kowloon Tong, Hong Kong

ARTICLE INFO

Article history:
Received 13 March 2019
Received in revised form
22 April 2019
Accepted 23 April 2019
Available online 25 April 2019

Keywords:
Metallopolymer
Synthesis
Characterization
Information storage
Write once read many times memory (WORM)

ABSTRACT

In this work, two metallopolymers (**P1** and **P2**) were designed and synthesized through coupling of ferrocene-anchored fluorene derivatives with porphyrin and benzene based diethynyl ligand, respectively. The chemical structure and physical properties of these two metallpolymers were fully characterized, which indicate that these two metallopolymers are thermally stable and semiconducting. Then, sandwich-like organic resistive memory based on **P1** and **P2** for data storage were explored. The memory device testing results manifest that both **P1** and **P2** are of the stable electric bistability and show write once read many times memory (WORM) characteristics.

1. Introduction

With the rapid development of economy and technology, human society has entered into the era of big data. It is reported that there will be over 40 trillion gigabytes of data generated by year 2020 [1,2]. Therefore, it is very urgent for the exploration of memory device with high density and specific characteristics, such as flexible, nonvolatile, high speed, low cost, *etc.* [3–5] In the past few decades, traditional inorganic materials especially the silicon-based semiconductors have been widely studied and applied in the every aspect of human daily life [6]. However, conventional silicon-based semiconductor devices are encountering severe downscaling constraints due to the poor data fidelity, heat death, and high cost, *etc.* [7,8] Moreover, flexible memories are extremely desired for constructing e-textiles, which can integrate us into internet electronic systems and facilitate our daily life [1,9,10]. Nevertheless, silicon-based semiconductor is intrinsically unsuitable for soft deformation scenario due to its primarily brittle electronic components. Therefore, design and physical realization of alternative information storage materials and devices operating on completely different mechanisms have attracted increasingly wide research interest and attention [11–14]. Among the new information storage materials and devices, organic materials-based resistive random access memory (RRAM or resistive switching memory) have been explored as the promising candidates for next-generation information storage technology, because the RRAM device has a simple sandwich-like structure with wide range of materials for selection and diverse switching mechanisms for flexible implementation. Moreover, diode structure of RRAM provides great potential to integrate into crossbar arrays with three-dimensional stacking architecture for high storage density [10,15,16].

Since the first discovery of resistive switching in amorphous oxides in the 1960s, a wide variety of organic, inorganic, and organic-inorganic hybrid materials have been explored to display resistive switching features [1,17,18]. Among them, organic polymer

* Corresponding author.
** Corresponding author.
E-mail addresses: dongqingchen@tyut.edu.cn (Q. Dong), val.roy@cityu.edu.hk (V.A.L. Roy).
[1] These people contribute equally to this work.

https://doi.org/10.1016/j.jorganchem.2019.04.025
0022-328X/

materials have gradually attracted more and more attention and made great progress because of their structure adjustable, light weight, low-cost fabrication as well as solution processability on various substrates, especially the soft substrates [19,20]. For example, Pan et al. successfully synthesized two D-A type polyazomethine (PAM) derivatives PAM-1 and PAM-2, and explored their memory applications by fabricating device through solution processing technology [21]. It is found that, PAM-1 shows rewritable bipolar resistive switching behavior, whereas PAM-2 exhibits only WORM resistive switching behavior. Chen and coworkers reported fabrication a flexible bipolar resistive switching memory with D-A conjugated polymer (PFT-PI) as a single active layer on plastic polyethylene naphthalate (PEN) substrate [22].

Compared with pure organic polymers, metallopolymers exhibit more abundant chemical and physical properties. In addition, the energy level of molecular orbital and energy gap can be easily adjusted by changing the metal species and ligand structures [23]. Ferrocene-containing polymers have become a research hotspot of metallopolymers due to the well-defined and stable electrochemical property of ferrocene moiety [24]. Choi and co-workers have reported a ferrocene-containing conjugated polymer (PFT2-Fc) which exhibits excellent nonvolatile multilevel storage characteristic due to the stability of ferrocene redox state (Fc^{3+}/Fc^{2+}) [25]. Tan and co-worker demonstrated a nonvolatile write-once-read-many times (WORD) memory by using four ferrocene-terminated hyperbranched polyimides. It is reported that switching mechanism was realized by the oxidation from ferrocene to ferrocenium ions [26]. In 2016, W. Y. Wong and coworkers reported four conjugated polymers by reacting ferrocene substituted fluorene derivative with four different π−conjugated aromatic moieties through Sonogashira coupling reaction [27]. It was found that structures of the main chains based on aromatic components make a huge impact on the memory device performance [27,28]. Therefore, the memory properties of the metallopolymers can be finely adjusted by changing the chemical structures of the backbones. Here, we reported the synthesis of two new conjugated ferrocene-containing metallopolymers and their organic nonvolatile memory applications due to the characteristics of electrical bistability.

2. Experimental

2.1. General information

All reactions were carried out under nitrogen unless otherwise stated. Commercially available reagents were used as received without further purification. All reactions were monitored by thin-layer chromatography (TLC) with Merck pre-coated glass plates. Compounds were visualized with UV light irradiation at 254 and 365 nm. Separation or purification of products was achieved by column chromatography or preparative TLC using silica gel from Merck (230–400 mesh). NMR spectra were measured in $CDCl_3$ on Bruker AV 400 or 600 NMR instrument with chemical shifts being referenced against tetramethylsilane as the internal standard for ^1H and ^{13}C NMR data. IR spectra were recorded on the Nicolet Magna 550 Series II FTIR spectrometer using KBr pellets for solid state spectroscopy. Thermal analyses were performed with a PerkinElmer TGA 6 thermal analyzer. The molecular weight of the polymer was determined by GPC using a HP 1050 series HPLC with visible wavelength and fluorescent detectors against polystyrene standards.

2.2. Synthesis of ferrocene-containing metallopolymers

2.2.1. Preparation of 4-(2-(trimethylsilyl)ethynyl)benzaldehyde (1)

In a 100 mL three-neck flask, 4-bromobenzaldehyde (1.5 g, 8.12 mmol), CuI (78 mg, 0.41 mmol) and $Pd(PPh_3)_4$ (270 mg, 0.23 mmol) were dissolved in solution of Et_3N (50 mL) at 0 °C. The mixture was stirred for 30 min, then trimethylsilylacetylene (8 mL, 56.6 mmol) were added to the three-neck flask. After reacting for 30 min, the mixture was heated to reflux for 12 h. The resulting mixture was collected and concentrated by a rotary evaporator. The crude material was purified by silica gel column chromatography using a mixture of petrol ether and DCM (v:v = 4:1) as the eluent to obtain the desired product as a yellow solid (785.3 mg, 47.8%). ^1H NMR (400 MHz, $CDCl_3$, δ/ppm): 10.00 (s, 1H, *CH*O), 7.85–7.83 (m, 2H, Ar-*H*), 7.61 (d, *J* = 8.0 Hz, 2H, Ar-*H*), 0.27 (s, 9H, TMS); ^{13}C NMR (125 MHz, $CDCl_3$, δ/ppm): 191.71, 135.74, 132.68, 129.66, 129.54, 104.01, 99.24, 77.45, 0.28 (TMS).

2.2.2. Preparation of compound (2)

In a 250 mL three-neck flask, meso-phenyldipyrromethane [29] (500 mg, 2.25 mmol), 4-((trimethylsilyl)ethynyl)benzaldehyde (455 mg, 2.25 mmol) and TFA (100 μL, 1.25 mmol) were dissolved in solution of DCM (100 mL). The mixture was stirred for 3 h at room temperature. 2,3-Dicyano-5,6-dichlorobenzoquinone (DDQ) (1.532 g, 6.75 mmol) were added to the three-neck flask. After reacting for 30 min, the resulting mixture was collected and concentrated by a rotary evaporator. The crude material was purified by silica gel column chromatography using a mixture of petrol ether and DCM (v:v = 4:1) as the eluent to obtain the desired product as a purple solid (170 mg, 17%). ^1H NMR (400 MHz, $CDCl_3$, δ/ppm): 8.81 (d, 8H, *J* = 8.0 Hz, Ar-*H*), 8.22–8.18 (m, 8H, Ar-*H*), 7.86 (d, *J* = 8.0 Hz, 4H, C=C*H*), 7.73 (d, *J* = 8.0 Hz, 6H, Ar-*H*), 0.38 (s, 18H, TMS), −2.80 (t, *J* = 8.0 Hz, 2H, *N*-*H*).

2.2.3. Preparation of compound (3)

In a 100 mL three-neck flask, compound **2** (100 mg, 0.124 mmol) and K_2CO_3 (20 mg) were dissolved in solution of DCM (20 mL) and methanol (20 mL). The mixture was stirred for 12 h at room temperature. The resulting mixture was extracted by dichloromethane for 3 times, and then the organic phase was collected and concentrated by a rotary evaporator. The crude material was purified by silica gel column chromatography using a mixture of petrol ether and DCM (v:v = 4:1) as the eluent to obtain the desired product as a purple solid (60.8 mg, 74%). ^1H NMR (600 MHz, $CDCl_3$, δ/ppm): 8.88 (d, *J* = 12.3 Hz, 8H), 8.26–8.20 (m, 8H), 7.93 (d, *J* = 7.1 Hz, 4H), 7.79 (d, *J* = 7.4 Hz, 6H), 3.35 (s, 2H), −2.75 (t, *J* = 8.3 Hz, 2H). IR (KBr): 3273 ($\upsilon_{C\equiv C\text{-}H}$) cm^{-1}; 2148 ($\upsilon_{C\equiv C}$) cm^{-1}.

2.2.4. Preparation of 1,4-bis(2-(trimethylsilyl)ethynyl)benzene (4)

The procedure for the preparation of 1,4-bis(2-(trimethylsilyl) ethynyl)benzene (**4**) was similar to that for compound **1**. The resulting product was obtained as a yellow solid (1.46 g, 85%). ^1H NMR (600 MHz, $CDCl_3$, δ/ppm): 7.38 (s, 4H), 0.25 (s, 18H).

2.3. Preparation of 1,4-diethynylbenzene (5)

The procedure for the preparation of 1,4-diethynylbenzene (**5**) was similar to that for compound **3**. The resulting product was obtained as a purple solid (443.3 mg, 95%). ^1H NMR (600 MHz, $CDCl_3$, δ/ppm): 7.44 (s, 4H), 3.17 (s, 2H).

2.4. Preparation of compound (6)

In a 100 mL three-neck flask, 2,7-diiodofluorene (418 mg, 1 mmol), ferrocenecarboxaldehyde (214 mg, 1 mmol) and KOH (2 g) were dissolved in solution of methanol (70 mL) under a nitrogen atmosphere. The mixture was heated to reflux for 3 h. The resulting mixture was extracted by dichloromethane for 3 times, and then the organic phase was collected and concentrated by a rotary evaporator. The crude material was purified by silica gel column

chromatography using petrol ether as the eluent to obtain the desired product as a red solid (583 mg, 95%). ^{1}H NMR (600 MHz, $CDCl_3$, δ/ppm): 8.60 (d, $J = 1.4$ Hz, 1H), 8.08 (d, $J = 1.3$ Hz, 1H), 7.68–7.64 (m, 2H), 7.45 (t, $J = 8.5$ Hz, 3H), 4.71 (t, $J = 1.8$ Hz, 2H), 4.57–4.56 (m, 2H), 4.26–4.24 (m, 5H).

2.5. Preparation of polymer P1

In a 100 mL three-neck flask, compound **3** (100 mg, 0.151 mmol) and compound **6** (92.6 mg, 0.151 mmol) were dissolved in solution of THF (20 mL) and NEt_3 (20 mL), followed by addition of CuI (2 mg) under a nitrogen atmosphere. The mixture was allowed to stir at room temperature for 24 h. Afterwards the solvent was removed by evaporation and the mixture was redissolved in a small amount of DCM (5 mL) and reprecipitated with the addition of methanol. Centrifugation was done to give a residual solid. The ferrocene-based metallopolymer **P1** was isolated as a red solid (180 mg, 94%). IR (KBr): 2193 ($\upsilon_{C\equiv C}$) cm^{-1}. GPC (THF): $M_w = 2782$, $M_n = 1986$, $M_w/M_n = 1.40$.

2.6. Preparation of polymer P2

Polymer **P2** was synthesized by reaction of compound **5** (20 mg, 0.151 mmol) and **6** (92.6 mg, 0.151 mmol). The preparation procedure is similar to that for **P1**. The final product was obtained as a red solid (105 mg, 96%). IR (KBr): 2203 ($\upsilon_{C\equiv C}$) cm^{-1}. GPC (THF): $M_w = 4143$, $M_n = 3821$, $M_w/M_n = 1.08$.

3. Results and discussion

3.1. Synthesis and characterization of the target metallopolymer

The synthetic routes of the target ferrocene-containing metallopolymers **P1** and **P2** were displayed in Scheme 1. The key intermediate of porphyrin derivative with diethynyl terminal groups was synthesized in the same way as reported by our group [30]. 1,4-dibromobenzene was used as starting material to generate the other diethynyl intermediate **5** through the similar synthetic reactions for compound **3**. Finally, the diethynyl derivatives **3** and **5**

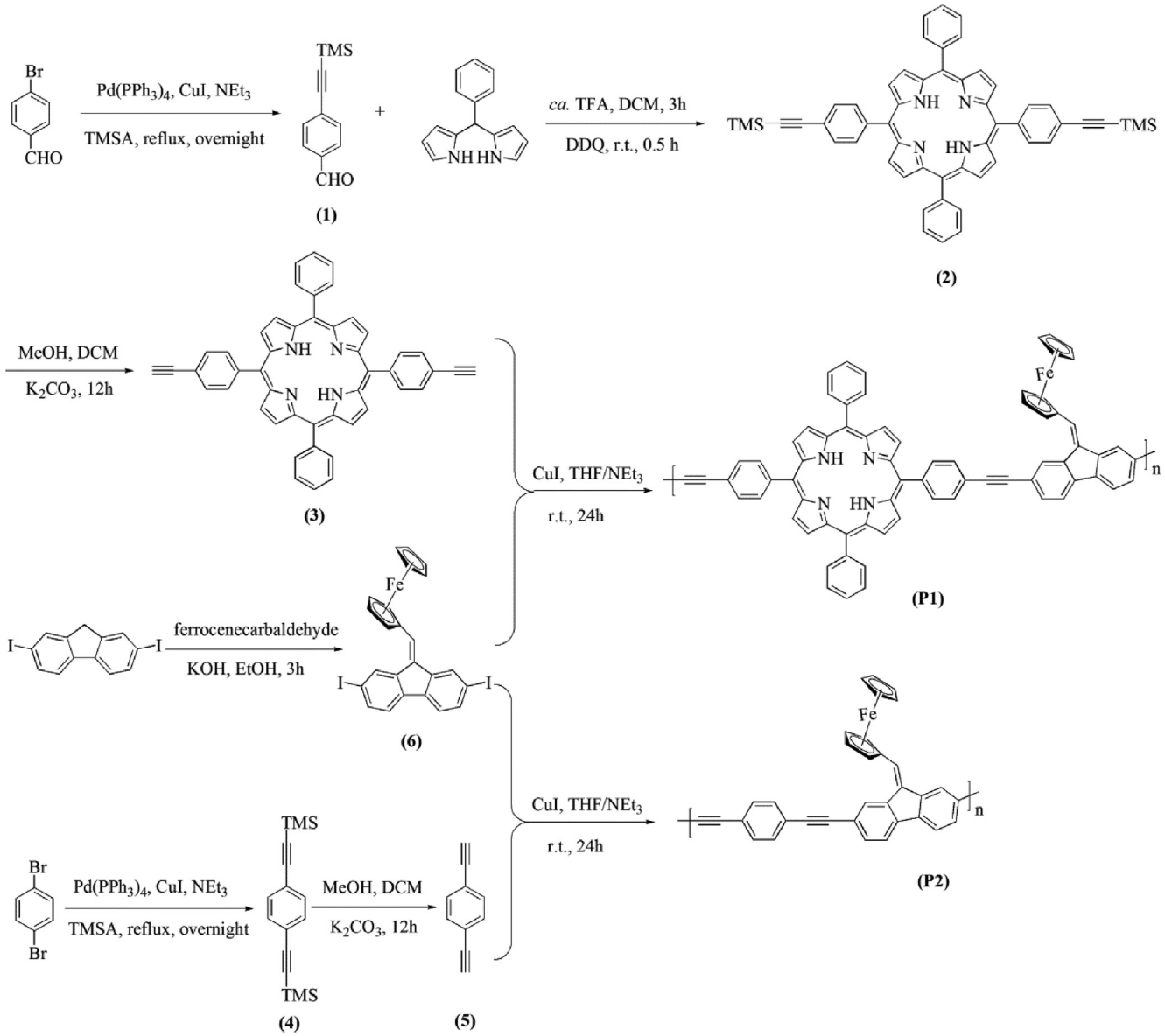

Scheme 1. Synthetic route of targeted metallopolymers **P1** and **P2**.

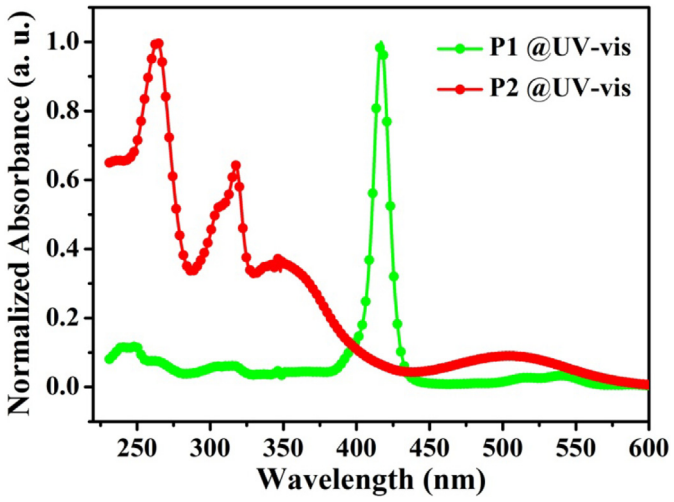

Fig. 1. Absorption spectra of **P1** and **P2** in dichloromethane solution at room temperature.

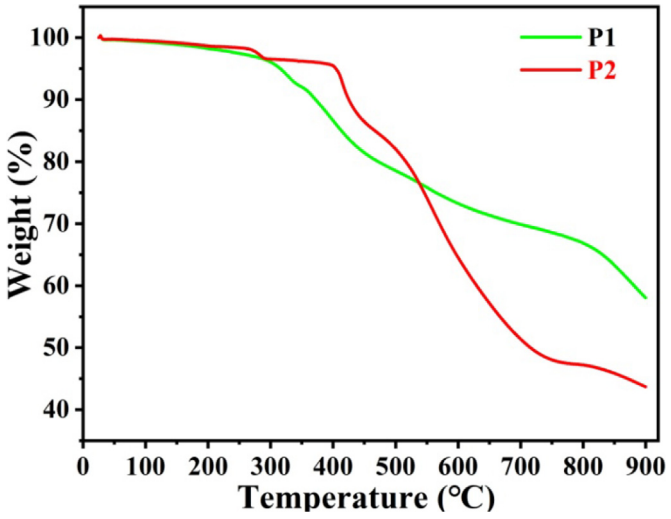

Fig. 2. TGA plots of **P1** and **P2** with a heating rate of 10 °C min^{-1} under N_2 atmosphere.

were allowed to couple with the ferrocene-containing diiodofluorene compound **6** through the Sonogashira coupling reaction to provide ferrocene-containing metallopolymers **P1** and **P2**, respectively. All these polymerization reactions proceeded with satisfactory yields and purified by repeated precipitation in a small amount of DCM from methanol for 2–3 times. The resulting polymers were well characterized by NMR, IR, GPC and TGA.

3.2. Optical and thermal properties

The optical features of **P1** and **P2** were investigated by UV–Vis absorption spectroscopy. Fig. 1 shows the normalized absorption spectra of the ferrocene-containing metallopolymers obtained in dichloromethane at room temperature. The intense absorption peaks of the porphyrin-coupled polymer are located at 417 nm, which is assigned to the $\pi \rightarrow \pi^*$ ($S_0 \rightarrow S_2$) transition [31]. While the benzyl-coupled polymer exhibits four sets of absorption peaks at 264, 320, 350 and 505 nm, respectively. The absorption peaks at around 264 nm correspond to the electronic transitions of the moiety of benzene in the conjugated polymer chains, while the peaks at around 320, 350 and 505 nm are assigned to the ferrocene-containing fluorene unit, which further proved the successful Sonogashira polycondensation [27]. The characteristic optical data is classified in Table 1.

The thermal stabilities of **P1** and **P2** were investigated by thermogravimetric analyses (TGA), which were performed by heating them to 900 °C at a rate of 10 °C min^{-1} under a nitrogen atmosphere. The decomposition temperature (T_d) of **P1** and **P2** are 320 and 407 °C, respectively with a weight loss of 5% (as shown in Fig. 2). The relative high decomposition temperature of **P2** may be attributed to its more rigid backbone structure. The high thermal stability is beneficial for long operating lifetime of the corresponding memory devices.

3.3. Electrochemical properties

To understand the electrochemical properties of **P1** and **P2** these two ferrocene-containing metallopolymers bearing different aromatic backbones, cyclic voltammetry (CV) measurements of **P1** and **P2** were undertaken in anhydrous dichloromethane (0.1 M tetra (n-butyl)ammoniumhexafluorophosphate as the supporting electrolyte; scan rate: 100 mV s^{-1}), with SCE reference electrode

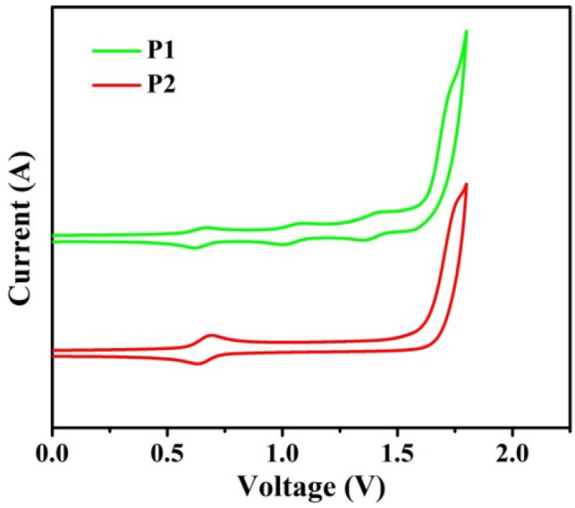

Fig. 3. Cyclic voltammograms of **P1** and **P2** in dichloromethane with tetra (n-butyl) ammoniumhexafluorophosphate (0.1 M) as the supporting electrolyte for the oxidation scan.

(ferrocene/ferrocenium (Fc/Fc^+) redox couple as the external standard), a glassy-carbon working electrode and a platinum-wire counter electrode. The onset oxidation potentials of **P1** and **P2** were measured to be 0.57 and 0.58 eV, respectively, from the cyclic voltammograms (as displayed in Fig. 3). The HOMO values for **P1** and **P2** were calculated to be −4.97 and −4.98 eV by the equation of $E_{HOMO} = -(E_{ox}\ (onset) + 4.4)$ eV. According to the formula $E_{LUMO} = E_{HOMO} + E_g$, the corresponding LUMO values of **P1** and **P2** were determined to be −2.17 and −2.92 eV [31].

3.4. Metallopolymer based organic memory devices

3.4.1. Device preparation

The polymer solutions were prepared by dissolving **P1** and **P2** (40 mg/mL) in 1,2-dichlorobenzene (DCB). The resulting solution was stirred for 1 h at 60 °C for obtaining a well-dissolved solution. Fig. 4 shows the device structure (Au/Polymer/ITO/Glass) of resistive memory devices. To obtain better reproducibility and higher surface coverage, ITO (indium tin oxide) coated glass substrate was

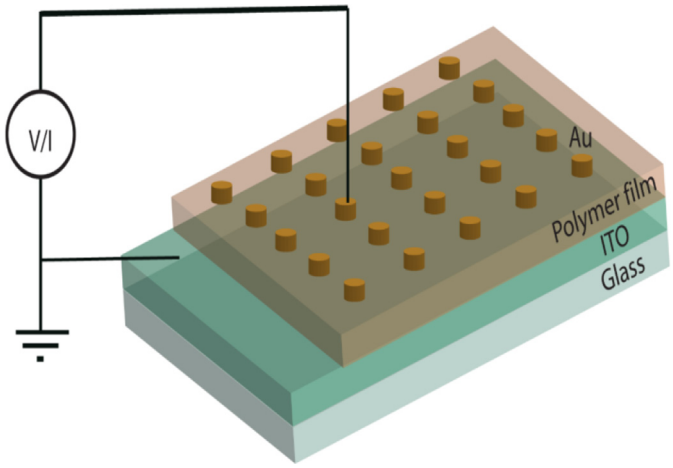

Fig. 4. Schematic of polymer film sandwiched between Au and ITO electrodes.

used as a bottom electrode for all the devices. For device fabrication, ITO coated glass substrates were successively cleaned in ultrasonic baths of Decon-90, acetone and deionized water for at least 30 min. The polymer solutions were filtered through a 0.2 μm PTFE membrane and spin coated on ITO coated glass substrates at 1000 rpm for 40 s followed by baking the substrate at 110 °C for 1 h. The thickness of the films was about 120 nm for **P1**, and 80 nm for **P2** measured via Ellipsometer. After that, Au-electrodes were deposited by thermal evaporation of 80 nm thick onto the polymer layer through a shadow mask at a rate of 0.1 $A^o\ s^{-1}$ to create memory cells with an area of $1.96 \times 10^{-4}\ cm^2$. The resulting devices based on **P1** and **P2** were recorded as **Device1** and **Device2**, respectively.

3.4.2. Organic memory behaviors

The current-voltage (I-V) curves of nonvolatile resistive memory devices are shown in Fig. 5 (a, b). The devices exhibit typical resistance switching characteristics under a direct voltage sweeping mode. The applied voltage is varied in a cycle from 0 V to +5 V–0 V to −5 V to 0 V with compliance current of 1 mA. During the first voltage sweep from 0 V to 5 V, the devices initially possess a high resistance state (HRS). These devices switch from HRS to low resistance state (LRS) at 2.5 V for **Device1**, and 1.5 V for **Device2** follows stage I, respectively, as a result, current increase abruptly (9.3551×10^{-4} to 0.03095 for **Device1** and 9.1217×10^{-4} to 0.0011 for **Device2**) follows stage II, corresponds to the SET process. When the voltage is swept back from 5 V to 0 V (stage III), the device kept at LRS. It is observed that the devices remain in its LRS state (SET process) during the subsequent negative voltage sweep stages (stage IV (0 V to −5 V) and stage V (−5 V to 0 V)), representing that the data cannot be erased after the writing process. Therefore, both **Device1** and **Device2** show write once read many times memory (WORM) characteristics, which exhibit stable non-volatile memory property with unipolar switching from HRS to LRS and the ON/OFF current ratios in the order of $<10^2$. The good stability in the LRS state is observed when the voltage swept (5 V to 0 V to -5 V) from stage III to stage IV representing the data cannot be erased after the writing process. The most significant features of these devices are the low resistance states does not go back to high resistance state by applying the subsequent negative voltage sweeps (Stage IV and Stage V) Therefore, these devices reveal WORM memory effect. The detailed device performances were summarized in Table 2. By analysis from the above CV curves, it can be learnt that **P2** shows higher peak current and larger slope (1.26 A and 7.24 for **P1**; 2.05 A and 15.7 for **P2**), implying its better reactivity and faster electron transfer kinetics [27]. Moreover, the LUMO energy level of **P2** is relatively lower than that of **P1**. The higher reactively, faster electron transfer kinetics as well as lower LUMO energy level of **P2**

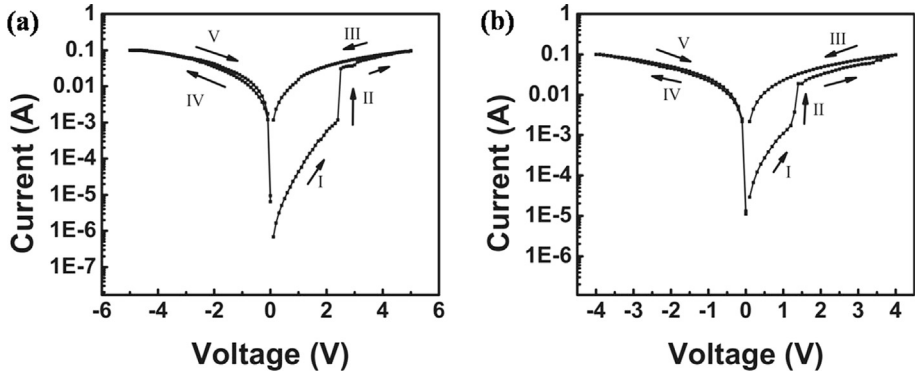

Fig. 5. The I-V curves of the RS behaviors of the Au/polymer/ITO WORM memory device. **(a) Device1** and **(b) Device2**.

Table 1
The physical properties of metallopolymers **P1** and **P2**.

Polymers	UV–vis (nm)[a]		E_g[b] (eV)	E_{ox} (onset)[c] (V)	HOMO[d]/LUMO[e] (eV)	T_g[f] (°C)
	λ_{max}	λ_{edge}				
P1	417	443	2.86	0.57	−4.97/-2.17	320
P2	264	505	2.06	0.58	−4.98/-2.92	407

[a] Measured in THF.
[b] Estimated from onset of the absorption spectra ($E_g = 1240/\lambda_{onset}$).
[c] Measured from cyclic voltammetry.
[d] Calculated from cyclic voltammetry.
[e] Calculated by the equation $E_{HOMO} = E_{LUMO} - E_g$.
[f] Measured by TGA.

Table 2
Summary of memory performance.

Device	Memory property	ON/OFF Ratio[a]	ON Voltage[a] (V_{set})	OFF Voltage (V_{reset})
Device1	WORM	27.29 (Read voltage = +1 V)	1.89 V	–
Device2	WORM	55.73 (Read voltage = +0.5 V)	1.54 V	–

[a] The error in ON/OFF ratio and ON voltage represents the standard deviation of the mean.

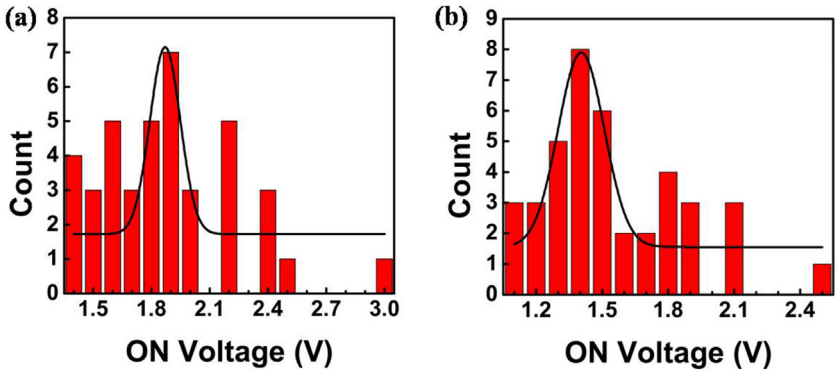

Fig. 6. Variation of ON voltages in **(a) P1** and **(b) P2** based RRAM devices.

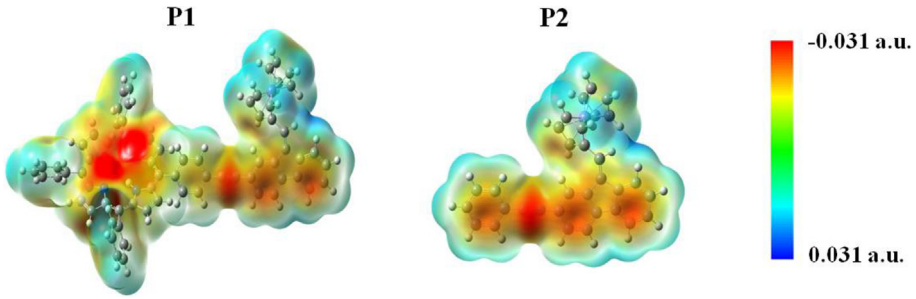

Fig. 7. Molecular simulation results for ESP surfaces of **P1** and **P2**.

contribute to the lower threshold voltage of the ON state of **Device2**. All above results indicate that the device based on polymer **P1** and **P2** behave as a write-once read many-times (WORM) device.

We also analyzed device-to-device reproducibility by measuring the set voltage for 40 devices for **P1** and **P2**. Fig. 6a–b shows the histogram of switch-on voltage for these two polymer WORM devices. The fabricated memory devices show nonvolatile low transition voltage with ON/OFF ratio $<10^2$. The standard deviation of the mean in the switch-on voltages of these devices is 1.89 ± 0.061 V for **P1** and 1.54 ± 0.050 V for **P2**. These data validate control over device-to-device as well as cycle-to-cycle stability.

3.4.3. Theoretical calculations

The electrical bistability of both **P1** and **P2** are mainly due to the well-known unique reversible and stable redox property of ferrocene, namely, both ferrocene (Fe^{2+}) and its oxidized form ferrocenium (Fe^{3+}) are extremely stable. This lays the foundation of nonvolatile memory property of the as-prepared ferrocene-containing metallopolymers. To gain deep insights into the memory behavior of **P1** and **P2**, theoretical electrostatic potential (ESP) were calculated by using density functional theory (DFT) molecular simulations. Fig. 7 shows the calculated ESP of **P1** and **P2**. It can be found that, the molecule surface has a continuous positive ESP (in red) along the conjugated backbone, indicating that a channel is formed from the molecular surface throughout the polymer backbone. This continuous channel is beneficial for the migration of charge carriers along the polymer backbone. Moreover, there are also negative ESP regions (in sky-blue) formed due to the electron-acceptor groups, which can serve as "traps" to impede the mobility of the charge carriers [32]. Therefore, the conjugated backbones of the polymers benefit for the transportation of charge carriers and regulate the threshold voltage of the ON state of memory devices.

4. Conclusions

In conclusion, we designed and synthesized two ferrocene-containing metallopolymers **P1** and **P2** in which ferrocene is covalently linked to the fluorene moiety as the side chain. Their structure, molecular weights, thermal and electrochemical properties and memory behaviors were fully characterized. The I-V characteristics of memory devices indicated the stable electric bistability of both **P1** and **P2**. Both two memory devices show WORM memory characteristics, which exhibit stable non-volatile memory property with unipolar switching from HRS to LRS and the ON/OFF current ratios in the order of $<10^2$. Further modification and optimization of materials and devices are still in progress.

Acknowledgements

We acknowledge the financial support from the National Natural Science Foundation of China (Grant No.: 61774109). This work

was also supported by the Youth "Sanjin" Scholar Program, the Key R&D Project of Shanxi Province (International cooperation program, No. 201603D421032), and the Natural Science Foundation for Outstanding Young Scientists of Shanxi Province, China (Grant No.: 201801D211007).

References

[1] S. Gao, X. Yi, J. Shang, G. Liu, R.-W. Li, Chem. Soc. Rev. (2018), https://doi.org/10.1039/c8cs00614h.
[2] J. Gantz, D. Reinsel. http://www.emc-technology.com/collateral/analyst-reports/idc-the-digital-universe-in-2020. pdf. (Accessed 25 July 2018).
[3] G.T. Meijer, Science 319 (2008) 1625–1626.
[4] H.S.P. Wong, S. Salahuddin, Nat. Nanotechnol. 10 (2015) 191–194.
[5] M. Ghoneim, M. Hussain, Electronics 4 (2015) 424–479.
[6] C. Li, D.H. Zhang, X.L. Liu, S. Han, T. Tang, C.W. Zhou, W. Fan, J. Koehne, J. Han, M. Meyyappan, A.M. Rawlett, D.W. Price, J.M. Tour, Appl. Phys. Lett. 82 (2003) 645–XXX.
[7] B. Cho, S. Song, Y. Ji, T.W. Kim, T. Lee, Adv. Funct. Mater. 21 (2011) 2806–2829.
[8] S. Song, B. Cho, T. W. Kim, Y. Ji, M. Jo, G. Wang, M. Choe, Y. H. Kahng, H. Hwang, T. Lee, 22 (2010) 5048–5052.
[9] S.-J. Liu, Z.-H. Lin, Q. Zhao, Y. Ma, H.-F. Shi, M.-D. Yi, Q.-D. Ling, Q.-L. Fan, C.-X. Zhu, E.-T. Kang, W. Huang, Adv. Funct. Mater. 21 (2011) 979–985.
[10] M. Ghoneim, M. Hussain, Electronics 4 (2015) 424–479.
[11] L.P. Ma, J. Liu, Y. Yang, Appl. Phys. Lett. 80 (2002) 2997–2999.
[12] Y.C. Yang, F. Pan, Q. Liu, M. Liu, F. Zeng, Nano Lett. 9 (2009) 1636–1643.
[13] M.-J. Lee, C.B. Lee, D. Lee, S.R. Lee, M. Chang, J.H. Hur, Y.-B. Kim, C.-J. Kim, D.H. Seo, S. Seo, U.I. Chung, I.-K. Yoo, K. Kim, Nat. Mater. 10 (2010) 625–630.
[14] Y. Shan, Z. Lyu, X. Guan, A. Younis, G. Yuan, J. Wang, S. Li, T. Wu, Phys. Chem. Chem. Phys. 20 (2018) 23837–23846.
[15] A. Sawa, Mater. Today 11 (2008) 28–36.
[16] Q.-D. Ling, D.-J. Liaw, C. Zhu, D.S.-H. Chan, E.-T. Kang, K.-G. Neoh, Prog. Polym. Sci. 33 (2008) 917–978.
[17] J. Choi, S.H. Ji, K. Hong, Y.K. Soo, W.J. Ho, Adv. Mater. 30 (2018) 1704002.
[18] T.W. Kim, Y. Yang, F. Li, W.L. Kwan, NPG Asia Mater. 4 (2012) e18.
[19] N. Gergel-Hackett, J.L. Tedesco, C.A. Richter, Proc. IEEE 100 (2012) 1971–1978.
[20] C.-L. Liu, W.-C. Chen, Polym. Chem. 2 (2011) 2169–2174.
[21] L. Pan, B. Hu, X. Zhu, X. Chen, J. Shang, H. Tan, W. Xue, Y. Zhu, G. Liu, R.-W. Li, J. Mater. Chem. C 1 (2013) 4556–4564.
[22] H.-C. Wu, A.-D. Yu, W.-Y. Lee, C.-L. Liu, W.-C. Chen, Chem. Commun. 50 (2014) 11496–11499.
[23] Q. Dong, Z. Meng, C.-L. Ho, H. Guo, W. Yang, I. Manners, L. Xu, W.-Y. Wong, Chem. Soc. Rev. 47 (2018) 4934–4953.
[24] P. Nguyen, P. Gómez-Elipe, I. Manners, Chem. Rev. 99 (1999) 1515–1548.
[25] T.-L. Choi, K.-H. Lee, W.-J. Joo, S. Lee, T.-W. Lee, M.Y. Chae, J. Am. Chem. Soc. 129 (2007) 9842–9843.
[26] H. Tan, H. Yu, Y. Song, S. Zhu, B. Zhang, H. Yao, S. Guan, J. Polym. Sci., Part A: Polym. Chem. 56 (2018) 505–513.
[27] J. Xiang, T.-K. Wang, Q. Zhao, W. Huang, C.-L. Ho, W.-Y. Wong, J. Mater. Chem. C 4 (2016) 921–928.
[28] J. Xiang, X. Li, Y. Ma, Q. Zhao, C.-L. Ho, W.-Y. Wong, J. Mater. Chem. C 6 (2018) 11348–11355.
[29] T. Gong, Z. Gao, W. Bian, F. Tai, W. Liang, W. Liang, Q. Dong, C. Dong, J. Organomet. Chem. 819 (2016) 237–241.
[30] Q. Dong, W. Qu, W. Liang, F. Tai, K. Guo, C.-W. Leung, W.-Y. Wong, J. Mater. Chem. C 4 (2016) 5010–5018.
[31] Q. Dong, H. Lian, Z. Gao, Z. Guo, N. Xiang, Z. Zhong, H. Guo, J. Huang, W.-Y. Wong, Dyes Pigments 137 (2017) 84–90.
[32] H. Li, Q. Xu, N. Li, R. Sun, J. Ge, J. Lu, H. Gu, F. Yan, J. Am. Chem. Soc. 132 (2010) 5542–5543.